EPJ Web of Conferences **290**, 02011 (2023) https://doi.org/10.1051/epjconf/202329002011
EuNPC 2022

Fission decay modes of ^{254}Fm* compound nucleus formed in ^{16}O+^{238}U reaction

Amandeep Kaur[1,*] and *Manoj* K. Sharma[2]

[1]Department of Physics, Faculty of Science, University of Zagreb, Bijenička c. 32, 10000 Zagreb, Croatia
[2]School of Physics and Materials Science, Thapar Institute of Engineering and Technology, 147004 Patiala, Punjab, India

Abstract. The quantum mechanical fragmentation theory (QMFT) based dynamical cluster-decay model (DCM) is applied to analyze the probable fission decay modes of ^{254}Fm* compound nucleus produced in ^{16}O+^{238}U nuclear reaction at excitation energy E^*_{CN}=45.9 MeV. The fission valley of collective fragmentation potential and the multi-humped peaks of preformation probability P_0 profile are analyzed by considering compact as well as elongated configurations of quadrupole (β_2) deformed fragments. The competitive emergence of different symmetric [symmetric superlong (SL), symmetric supershort (SS)] and asymmetric [standard 1 (S1), standard 2 (S2), standard 3 (S3)] fission modes have been observed for the case of elongated configuration. The division of mass and charge in nuclear fission of ^{254}Fm* depicts the importance of spherical and deformed magic shell closures. The most energetic light (A_L and heavy (A_H) decay fragments of aforementioned fission modes are identified. Moreover, the DCM-calculated fission cross-sections ($\sigma_{fission}$) show reasonable agreement with the experimental measurements [24].

1 Introduction

The nuclear fission process is crucial not only for the experimental and theoretical nuclear/astrophysics studies, but also for the production of energy and exotic nuclear isotopes that are useful in the medical and industrial applications. In a broader scenario, a fissioning nucleus disintegrates in either a symmetric or asymmetric fission mode. However, there may be a possibility of multimodal fission, during which a fissioning nucleus may choose different decay paths such as symmetric superlong (SL), symmetric supershort (SS), asymmetric standard 1 (S1), asymmetric standard 2 (S2), asymmetric standard 3 (S3) and superasymmetric (SA), for description see [1]. The proton (Z) and neutron (N) number of such fission fragments are determined by the shell effects. The predominance of asymmetric fission mode has been seen in the nuclear elements of actinide region [2]. The primary observation of a transition from asymmetric to symmetric fission has been measured in the region of mass A=254-258 of Fm isotopes [3, 4]. Similar kind of results have been predicted lately in the fission decay of ^{254}Es nucleus [5]. It is indeed highly desirable to investigate the nuclear fission near mass 254 due to the interplay among symmetric and asymmetric fission decay paths.

It is well known that macroscopic and microscopic effects impart a substantial impact on the emergence of symmetric and asymmetric fission of a nucleus, but in addition, the deformation and orientation of decay fragments also influence the fission fragment mass distribution [1, 6]. The side-to-side (polar or compact) and tip-to-tip (equatorial or elongated) configurations of nuclei have great impact on the formation and decay dynamics of a nucleus [7]. Recently, we have made an effort to see the effect of compact and elongated configurations of quadrupole (β_2) deformed decay fragments on the spontaneous fission of $^{242-260}$Fm isotopes using preformed cluster model [8]. It has been observed that tip-to-tip (elongated) configuration results in the production of double-peaked (asymmetric) to triple-humped (multimodal) fission fragment mass distribution with increase in neutron number of Fm isotopes.

In the present work, quantum mechanical fragmentation theory (QMFT) [9] based dynamical cluster-decay model (DCM) [10, 11] is applied to analyze the possibility of multimodal fission mode of excited ^{254}Fm* compound nucleus (CN) formed in ^{16}O+^{238}U nuclear reaction. The calculations are made at center-of-mass energy $E_{c.m.}\approx$84 MeV (excitation energy E^*_{CN}=45.9 MeV) near the Coulomb barrier by considering quadrupole β_2-deformed nuclei having compact/elongated configurations with optimum orientations ($\theta_i^{opt.}$) [7]. The temperature (T) dependence is included in β_2-deformations (called as β_2-dynamic deformation), as explained in section 2. The objectives of this work is (i) to examine the different fission decay paths of ^{254}Fm* nucleus by analyzing the valleys of collective fragmentation potential $V_R(\eta$,T) and peaks of preformation probability P_0 of fission fragments; (ii) to study the role of compact and elongated orientations of β_2-deformed fragments on the structure of fission fragment mass distribution; (iii) to predict the energetically favorable light (A_L) and heavy (A_H) fission fragments in order to see the role of spherical and deformed magic shell

*Corresponding author: akaur.phy@pmf.hr

closure; and (iv) a comparison of DCM-calculated results with the recent experiment measurements [12].

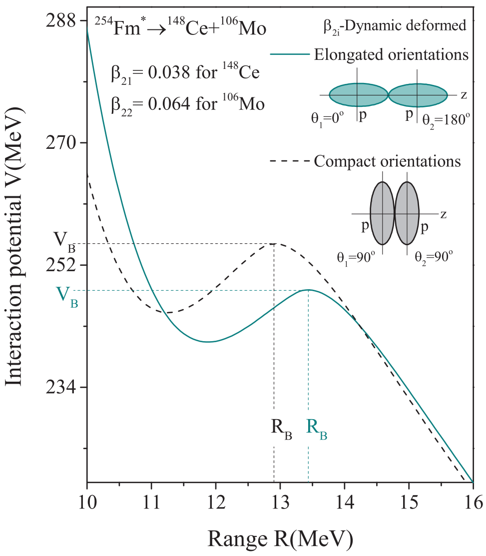

Figure 1. The interaction *or* scattering potential V(R) is plotted for asymmetric fission channel $^{254}Fm^{*}\rightarrow^{148}Ce+^{106}Mo$ using both β_2-dynamic elongated and compact configurations.

2 Methodology or Formalism

Various fission channels of $^{254}Fm^{*}$ CN are studied using dynamical cluster-decay model (DCM) [10, 11], which in terms of collective coordinates of mass (and charge) asymmetries $\eta_A = (A_1-A_2)/(A_1+A_2)$ (and $\eta_Z = (Z_1-Z_2)/(Z_1+Z_2)$) (where 1 and 2 stand for heavy (A_H) and light (A_L) fragments), relative separation R, the multipole deformations $\beta_{\lambda i}$ (λ=2, 3, 4; i=1, 2) and orientations θ_i (i=1, 2). Using these collective coordinates, the combine effect of attractive and repulsive interactions on a decay process is explored in terms of fragmentation potential $V_R(\eta,T)$ as

$$\begin{aligned} V_R(\eta,T) &= \sum_{i=1}^{2}[V_{LDM}(A_i,Z_i,T)] \\ &+ \sum_{i=1}^{2}[\delta U_i]exp(-T^2/T_0^2) \\ &+V_C(R,Z_i,\beta_{\lambda i},\theta_i,T) \\ &+V_P(R,A_i,\beta_{\lambda i},\theta_i,T) \\ &+V_\ell(R,A_i,\beta_{\lambda i},\theta_i,T). \end{aligned} \quad (1)$$

The V_C, V_P and V_ℓ are respectively, the T-dependent Coulomb, the nuclear proximity and centrifugal potentials for deformed and oriented nuclei [13]. The prox1977 version of the V_P [14] is considered for the calculations. V_{LDM} is T-dependent liquid drop energy of Davdison et al. [15] and δU, the “empirical" shell correction, as given in [16], made T-dependent as per [17]. The constants of V_{LDM} at T=0 are refitted [13] to give the experimental binding energies of Audi et al. [18] or the theoretical estimates of Möller et al. [19] if not available in [18]. The quadrupole deformations (β_{2i}) are taken from the theoretical estimates of Möller et al. [19], and the "optimum" orientations $\theta_i^{opt.}$ for hot-compact and cold-elongated configurations are taken from Table 1 of Ref. [7]. The temperature effects are included in deformation parameters using following relation [20, 21], $\beta_{\lambda i}(T) = exp(-T/T_0)\beta_{\lambda i}(0)$, where $\beta_{\lambda i}(0)$ represents the static deformation and T_0 is the temperature of the nucleus at which shell effects start to vanish (T_0 = 1.5 MeV) [17]. The nuclear temperature (T) is related to CN excitation energy as $E^*_{CN} = E_{c.m.} + Q_{in} = (A_{CN}/9)T^2 - T$, where Q_{in} is the Q-value of entrance channel. To study the fragment mass distribution and energetically favoured nascent fragments, the preformation probability P_0 is calculated using the fragmentation potential $V_R(\eta,T)$ by solving the Schrödinger equation in η-coordinate at fixed $R = R_a$,

$$\left\{-\frac{\hbar^2}{2\sqrt{B_{\eta\eta}}}\frac{\partial}{\partial\eta}\frac{1}{\sqrt{B_{\eta\eta}}}\frac{\partial}{\partial\eta} + V(\eta,R,T)\right\}\psi^\nu(\eta) = E^\nu\psi^\nu(\eta), \quad (2)$$

with $\nu = 0, 1, 2, 3...$ referring to ground state ($\nu = 0$) and excited state solutions, with the ground state P_0 given as

$$P_0 = |\psi(\eta(A_i))|^2\sqrt{B_{\eta\eta}}\frac{2}{A_{CN}}, \quad (3)$$

and $|\psi|^2 = \sum_{\nu=0}^{\infty}|\psi^\nu|^2 exp(\frac{-E^\nu}{T})$ is Boltzmann-like function. $B_{\eta\eta}$ in Eq. (3) represent the smooth hydrodynamical mass parameter [22]. The penetration probability P of decaying fragments is calculated using Wenzel-Kramers-Brillouin integral. The first turning point of penetration path is defined as $R_a(T) = R_1(\alpha_1,T)+R_2(\alpha_2,T)+\Delta R(T) = R_t(\alpha,T) + \Delta R(T)$, with radius vectors R_i (i = 1, 2)

$$R_i(\alpha_i,T) = R_{0i}(T)\left[1 + \sum_\lambda \beta_{\lambda i}Y_\lambda^{(0)}(\alpha_i)\right] \quad (4)$$

and T-dependent nuclear radii R_{0i} of the equivalent spherical nuclei [23], $R_{0i}(T) = [1.28A_i^{\frac{1}{3}} - 0.76 + 0.8A_i^{\frac{-1}{3}}](1 + 0.0007T^2)fm$. ΔR is the only parameter of the model known as neck-length parameter. Using P_0 and P, for ℓ partial waves, the decay and fragment's production cross-section is given by

$$\sigma(A_1,A_2) = \frac{\pi}{k^2}\sum_{\ell=0}^{\ell_{max}}(2\ell+1)P_0P; \quad k = \sqrt{\frac{2\mu E_{c.m.}}{\hbar^2}}, \quad (5)$$

where $\mu = m[A_1A_2/(A_1 + A_2)]$ is the reduced mass, and ℓ_{max} is maximum angular momentum fixed for the vanishing of light particle cross sections.

3 Results and Discussions

Figure 1 shows the scattering potential V(R) for the asymmetric fission channel $^{254}Fm^{*}\rightarrow^{148}Ce+^{106}Mo$ for β_2-dynamic elongated and compact configurations at ℓ=0$\hbar$. The heavy A_H and light A_L fission fragments ^{148}Ce and ^{106}Mo are prolate in shape. Depending on the prolate (p) and oblate (o) shapes (+ and - signs) of β_{2i} deformations, the orientation angles are uniquely fixed, which result in the “hot-compact" and “cold-elongated" configurations [7], a pictorial representation is shown in the figure. It is observed from the figure that barrier properties

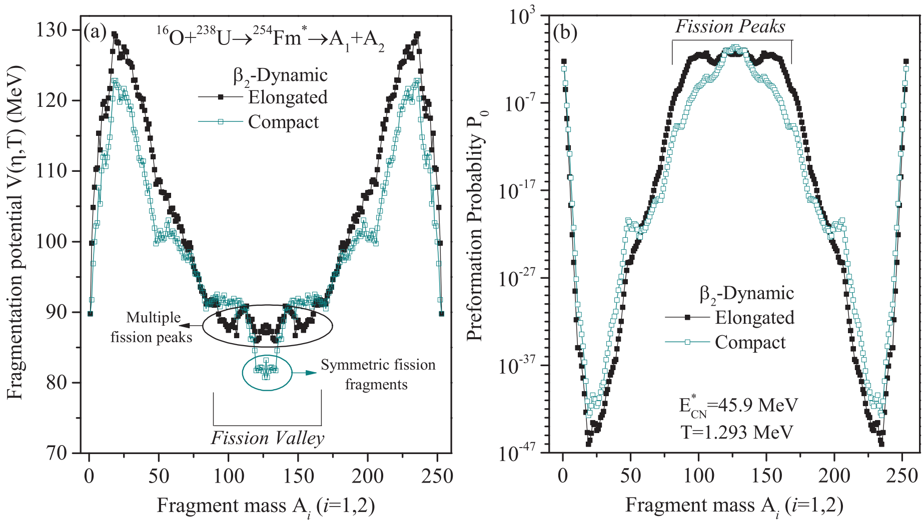

Figure 2. DCM-calculated (a) collective fragmentation potential $V_R(\eta, T)$ and (b) preformation probability P_0 as a function of fragment mass A$_i$ (i=1,2) of ^{254}Fm* at E^*_{CN}=45.9 MeV are plotted for β_2-dynamic deformations for elongated and compact configurations.

Table 1. DCM-calculated and experimental [24] $\sigma_{fission}$ of ^{254}Fm* formed in ^{16}O+^{238}U reaction at E^*_{CN}=45.9 MeV for β_2-deformed compact and elongated configurations.

Orientation	ΔR (fm)	ℓ_{max} ($\hbar$)	Fragments (A$_2$)	$\sigma^{DCM}_{fission}$ (mb)	$\sigma^{Expt.}_{fission}$ (mb)
Elongated	0.854	156	85-127	115.4	118.5
Compact	0.900	142	95-127	120.8	

are significantly modified with change in orientation criteria. The barrier height (V_B) is small and barrier position (R_B) is large for the case of elongated configuration as compared to the compact one. This suggests that using distinct methods of orientations the fragmentation potential V$_R$(η,T) and preformation probability P_0 get modified, and hence elongated and compact orientations impact on the fission dynamics significantly. Further, table 1 shows the DCM calculated fission cross-sections ($\sigma_{fission}$) along with other related quantities for the most probable fission fragments (A$_1$+A$_2$) of ^{254}Fm* nucleus at E^*_{CN}=45.9 MeV, which are calculated by fixing neck-length parameter ΔR for both elongated and compact fragment configurations. The calculated $\sigma_{fission}$ show nice agreement with experimental data given in [24].

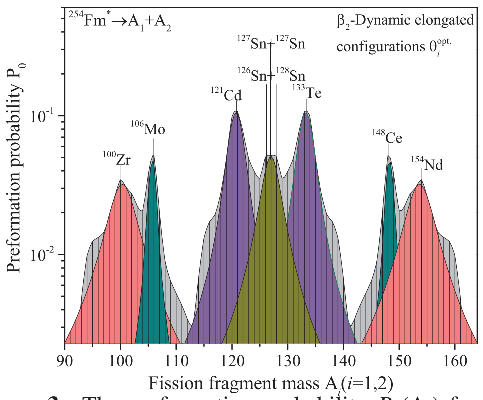

Figure 3. The preformation probability P_0(A$_i$) for the fission mass region of ^{254}Fm* is plotted for elongated configurations.

For the analysis of fission valleys, the fragmentation potential V$_R$(η,T) of ^{254}Fm* is plotted as a function of fragment mass A$_i$(i=1,2) at E^*_{CN}=45.9 MeV and ℓ_{max}-value in figure 2(a) for β_2-deformed elongated as well as compact approach. The first look of fragmentation potential suggests relatively more structural effects in the fission valley of tip-to-tip elongated configurations in contrast to side-to-side compact configuration. The fission dips of compact interactions show the dominance of symmetric fission fragments whereas the elongated configurations depict the multiple dips, which point towards the possibility of the co-existence of various fission decay channels for ^{254}Fm* CN. Next, figure 2(b) represents the preformation probability P_0(A$_i$) of ^{254}Fm* at E^*_{CN}=45.9 MeV and ℓ_{max}-value for both elongated and compact orientations. Note that the fragmentation potential goes as an input in the Schrödinger equation used to calculate the preformation probability P_0, and the minima of the fragmentation potential correspond to the maxima of the preformation probability and vice versa, as evident from figures. 2(a) and 2(b). The symmetric peak becomes sharp for the compact orientations while multi-humped fission fragment mass distribution is observed for the case of elongated configurations. This means β_2-deformed compact and elongated configurations follow different fission decay paths. According to recent experimental and theoretical observation of [12], the fragment mass distribution of ^{254}Fm* at excitation energy E^*_{CN}≈45 MeV may decompose into different fission paths. Therefore, it would be interesting to analyze the energetically favoured fission peaks of preformation probability for elongated oriented fission fragments in DCM calculations, which indicates the possibility of competing fission decay paths.

To explore the multiple fission decay paths of ^{254}Fm* at E^*_{CN}=45.9 MeV and ℓ_{max}-value, a broader representation of preformation probability P_0 as a function of fission fragment mass is represented in figure 3 for the elongated fragment configurations. Several symmetric and asymmetric fission decay modes as described in [1] are marked in figure and represented in table 2 along with experimentally observed heavy fission mass fragments A$_H$. Note that

Table 2. DCM-predicted light A_L and heavy A_H fission fragments in several fission decay channels of ^{254}Fm* nucleus at E^*_{CN}=45.9 MeV are presented along with the experimental observations of [12].

Fission mode	Heavy mass fission fragment A_H	Light mass fission fragment A_L	A_H [12]
Symmetric superlong (SL)	^{127}Sn(Z_H=50, N_H=77); (β_2=0.0)	^{127}Sn(Z_L=50, N_L=77); (β_2=0.0)	127.00
	^{128}Sn(Z_H=50, N_H=78); (β_2=0.0)	^{126}Sn(Z_L=50, N_L=76); (β_2=0.0)	
Asymmetric Standard 1 (S1)	^{133}Te(Z_H=52, N_H=81); (β_2=0.001)	^{121}Cd(Z_L=48, N_L=73); (β_2=0.024)	135.00
Asymmetric Standard 2 (S2)	^{148}Ce(Z_H=58, N_H=90); (β_2=0.038)	^{106}Mo(Z_L=42, N_L=64); (β_2=0.064)	143.00
	^{154}Nd(Z_H=60, N_H=76); (β_2=0.048)	^{100}Zr(Z_L=40, N_L=60); (β_2=0.064)	
Asymmetric Standard 3 (S3)	^{159}Sm(Z_H=62, N_H=97); (β_2=0.052);	^{95}Sr(Z_L=38, N_L=57); (β_2=0.055)	163.61±1.46

deformations mentioned in the table are T-dependent. The symmetric superlong SL fission channel is mainly situated near $A_{CN}/2$ i.e. A_H=127, 128 and both fission decay fragments are spherical in shape. This fission mode is mainly defined by the macroscopic liquid drop part of fragmentation potential. Standard S1 and S2 are asymmetric fission paths which can be found at either side of the symmetric hump. Generally, the S1 and S2 modes are situated at A_H=132-135 and A_H=138-144, respectively and at neutron shell closures N_H=82 (spherical) and $N_H \approx 88$ (deformed), respectively. Similar results we have observed in DCM calculations. S1 mode has one spherical heavy fragment and a deformed light fragment and for S2 mode we have observed two deformed prolate fragments. For asymmetric S3 fission mode, the role of deformed magic shell closures of Z_L=38 and N_L=60 can be seen. The DCM predicted heavy and light fission fragment mass numbers show reasonable agreement with the previous experimental and theoretical observations [1, 2, 12]. Hence, the deformations, oreintations and shell effects play significant role in the splitting of a nucleus. However, for the present study the deformations are used up to quadrupole only and it would be interesting to see the effect of octupole deformations of fragments in the fission process as stabilized octupole configuration around Z=52 and 56 is supposed to play important role in the splitting of a fissioning nucleus.

4 Summary

Summarizing, the ^{16}O-induced fission of ^{254}Fm* is studied within the framework of dynamical cluster-decay model (DCM) at excitation energy E^*_{CN}=45.9 MeV. The scattering potential V(R), collective fragmentation potential $V_R(\eta,T)$ and preformation probability P_0 are computed for two type of decay fragment orientations: elongated and compact. The barrier characteristics have been considerably modified in terms of barrier height (V_B) and barrier position (R_B) with change in orientation degree of freedom. The fragmentation potential represents more structure in elongated interaction as compared to compact one. Hence, multiple peaks are observed in preformation probability distribution for elongated case, which indicates the possibility of different fission decay modes for ^{254}Fm* nucleus. These results are in agreement with the available data. Spherical/deformed magic shell closures play significant role in the division of fissioning nuclei. It would be interesting to include the pear shaped deformations in the decaying fragments for the case of elongated orientations, to analyse the role of deformed shell closures in fission modes of ^{254}Fm* and nearby nuclei.

5 Acknowledgements

This work is supported by the QuantiXLie Centre of Excellence, a project co-financed by the Croatian Government and European Union through the European Regional Development Fund, the Competitiveness and Cohesion Operational Programme (KK.01.1.1.01.0004). MKS is thankful to DST-SERB project grant CRG/2021/001144.

References

[1] U. Brosa, S. Grossmann, A. Müller, Phys. Rep. **197**, 167 (1990)

[2] K. Mahata, C. Schmitt, Shilpi Gupta, A. Shrivastava, G. Scamps, K.-H. Schmidt, Phys. Lett. B **825**, 136859 (2022)

[3] E. K. Hulet et al., Phys. Rev. C **40**, 770 (1989)

[4] J. E. Gindler, K. F. Flynn, L. E. Glendenin, R. K. Sjoblom, Phys. Rev. C **16**, 1483 (1977)

[5] M. D. Usang, F. A. Ivanyuk, C. Ishizuka, S. Chiba, Sci. Rep. **9**, 1525 (2019)

[6] K. Nishio, H. Ikezoe, S. Mitsuoka, I. Nishinaka, Y. Nagame, Y. Watanabe, T. Ohtsuki, K. Hirose, S. Hofmann, Phys. Rev. C **77**, 064607 (2008)

[7] R. K. Gupta, M. Balasubramaniam, R. Kumar, N. Singh, M. Manhas, W. Greiner, J. Phys. G: Nucl. Part. Phys. **31**, 631 (2005)

[8] A. Kaur, N. Sharma, M. K. Sharma, Phys. Rev. C **103**, 034618 (2021)

[9] R. K. Gupta, W. Scheid, W. Greiner, Phys. Rev. Lett. **35**, 353 (1975)

[10] A. Kaur, M. K. Sharma, Phys. Rev. C **99**, 044611 (2019)

[11] A. Kaur, M. K. Sharma, Eur. Phys. J. A **55**, 89 (2019)

[12] T. Banerjee et al., Phys. Rev. C **105**, 044614 (2022)

[13] B. B. Singh, M. K. Sharma, R. K. Gupta, Phys. Rev. C **77**, 054613 (2008)

[14] R. Kumar, M. K. Sharma, Phys. Rev. C **85**, 054612 (2012)

[15] N. J. Davidson, S. S. Hsiao, J. Markram, H. G. Miller, Y. Tzeng, Nucl. Phys. A **570**, 61 (1994)

[16] W. Myers, W. J. Swiatecki, Nucl. Phys. **81**, 1 (1966)

[17] A. S. Jensen, J. Damgaard, Nucl. Phys. A **203**, 578 (1973)

[18] G. Audi, A. H. Wapstra, C. Thibault, Nucl. Phys. A **729**, 337 (2003)

[19] P. Möller, J. R. Nix, W. D. Myers, W. J. Swiatecki, At. Data Nucl. Data Tables **59**, 185 (1995)

[20] M. Rashdan, A. Faessler, W. Waida, J. Phys. G: Nucl. Part. Phys. **17**, 1401 (1991)

[21] M. Muenchow, W. Scheid, Phys. Lett. B **162**, 265 (1985); Nucl. Phys. A **468**, 59 (1987)

[22] H. Kröger, W. Scheid, J. Phys. G: Nucl. Part. Phys. **6**, L85 (1980)

[23] G. Royer, J. Mignen, J. Phys. G: Nucl. Part. Phys. **18**, 1781 (1992)

[24] H. Zhang, Z. Liu, J. Xu, X. Qian, Y. Qiao, C. Lin, K. Xu, Phys. Rev. C **49**(2), 926 (1994)